Solar Energy Materials & Solar Cells 121 (2014) 35–41

Contents lists available at ScienceDirect

Solar Energy Materials & Solar Cells

journal homepage: www.elsevier.com/locate/solmat

Solution-processable bismuth iodide nanosheets as hole transport layers for organic solar cells

Karunakara Moorthy Boopathi [a,b,c], Sankar Raman [d], Rajeshkumar Mohanraman [a,b,e], Fang-Cheng Chou [d], Yang-Yuang Chen [e], Chih-Hao Lee [b], Feng-Chih Chang [f,g], Chih-Wei Chu [c,h,*,1]

[a] Nanoscience and Technology Program, Taiwan International Graduate Program, Academia Sinica, Taipei 115, Taiwan
[b] Department of Engineering and Systems Science, National Tsing Hua University, Hsinchu 30013, Taiwan
[c] Research Center for Applied Science, Academia Sinica, Taipei 115, Taiwan
[d] Center for Condensed Matter Sciences, National Taiwan University, Taipei 10617, Taiwan
[e] Institute of Physics, Academia Sinica, Taipei 115, Taiwan
[f] Department of Materials and Optoelectronic Science, National Sun Yat-Sen University, Kaohsiung 80424, Taiwan
[g] Center for Membrane Technology, Chung Yuan Christian University, Chungli, Taoyuan 32043, Taiwan
[h] Department of Photonics, National Chiao Tung University, Hsinchu, 300, Taiwan

ARTICLE INFO

Article history:
Received 6 June 2013
Received in revised form
23 August 2013
Accepted 27 October 2013
Available online 15 November 2013

Keywords:
Bismuth iodide nanosheet
Hole transport layer
Low temperature
Solution-processable
Organic photovoltaics

ABSTRACT

In this paper we demonstrate the use of low-temperature-solution-processable bismuth iodide (BiI_3) nanosheets as hole transport layers in organic photovoltaics with an active layer comprising poly(3-hexylthiophene) (P3HT) mixed with a fullerene derivative. The performance of the resulting devices was comparable with that of corresponding conventionally used systems incorporating polyethylenedioxythiophene:polystyrenesulfonate (PEDOT:PSS). UV–vis spectroscopy revealed that the transparency of a BiI_3 layer in the visible (> 620 nm) and near-infrared range is greater than that of a PEDOT:PSS layer. X-ray photoemission spectroscopy of a BiI_3 film revealed signals at 158.8, 164, 618.6, and 630 eV—characteristic of Bi $4f_{7/2}$, Bi $4f_{5/2}$, I $3d_{5/2}$, and I $3d_{3/2}$, respectively—that indicated a stoichiometric BiI_3 film. Wet milling of BiI_3 crystals resulted in the formation of nanosheets, the presence of which we confirmed using scanning electron microscopy. The resultant power conversion efficiency of the device was approximately 3.5%, with an open-circuit voltage of 0.56 V, a short-circuit current density of 10.4 mA cm^{-2}, and a fill factor of 60.1% under AM1.5G irradiation (100 mW cm^{-2}).

1. Introduction

Harnessing natural energy might be the best approach toward satisfying today's growing world energy demands, with solar energy the undisputed frontrunner among all such sources. Organic photovoltaics (OPVs) based on polymeric materials are promising candidates for harvesting solar energy for various reasons, including simple solution-processability, light weight [1], mechanical flexibility and transparency [2,3], and the ability to produce solar panels on large scale at low cost [4–6]. In particular, solution-processed bulk heterojunction (BHJ) solar cells are receiving much attention because of their superior mechanical robustness, easy blending, and high power conversion efficiencies (PCEs). Devices incorporating blends of regioregular poly(3-hexylthiophene) (P3HT) as the electron donor and phenyl C_{61}-butyric acid methyl ester (PCBM), a soluble fullerene derivative, as the acceptor have reached PCEs of 3–5% [7,8]. P3HT forms long, thin conducting nanowires and PCBM forms more-homogeneous nanocrystalline films when annealed. The importance of annealing during processing cannot be overestimated; it increases phase separation, crystallization, and the photophysical and transport properties of the active layer [7].

A buffer layer is an important constituent between the electrode and active layer; it plays the crucial role of extracting and transporting the photogenerated carriers (holes or electrons). While it allows movement of one kind of the carrier, it blocks the passage of the other through an energy mismatch, often resulting in a dramatic increase in PCE [9–11]. Polyethylenedioxythiophene:polystyrenesulfonate (PEDOT:PSS) is used widely as a standard anode buffer layer as well as standalone indium tin oxide (ITO)-free anode in OPVs because of its excellent transporting properties, high transparency, and smooth textured surface [12–15]. Nevertheless, because of its acidic and hygroscopic nature, PEDOT:PSS can interact physically and chemically with adjoining layers, thereby degrading device performance [16,17]. In the quest for replacements for

* Corresponding author: Chih-Wei Chu at Research Center for Applied Science, Academia Sinica, Taipei 115, Taiwan.
E-mail address: gchu@gate.sinica.edu.tw (C.-W. Chu).
[1] http://www.rcas.sinica.edu.tw/faculty/gchu.html.

0927-0248/$ - see front matter © 2013 Elsevier B.V. All rights reserved.
http://dx.doi.org/10.1016/j.solmat.2013.10.031

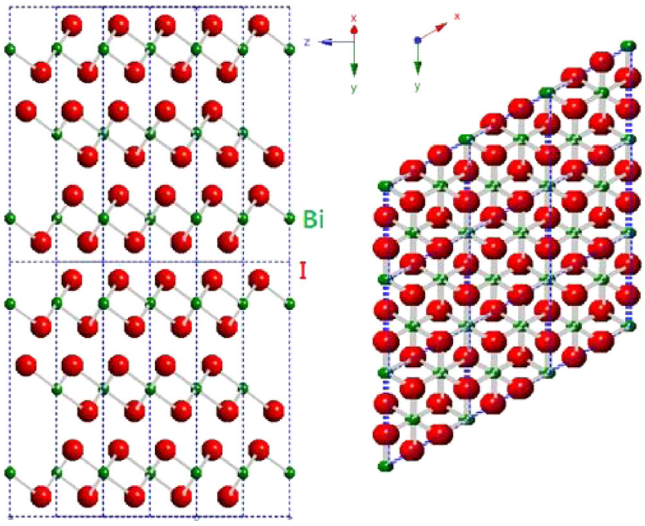

Fig. 1. Crystal structure of BiI_3; the Bi and I atoms are displayed as green and red spheres, respectively. (For interpretation of the references to color in this figure legend, the reader is referred to the web version of this article.)

PEDOT:PSS, researchers have identified various metal oxide hole transport materials such as tungsten oxide (WO_3) [18–20], molybdenum oxide (MoO_3) [20–22], nickel oxide (NiO_x) [23], and vanadium oxide (V_2O_5) [20,24] for OPVs with improved device performance. However, these materials require stringent conditions of high vacuum, high temperature processing and high power consumption which increases the resulting cost of fabrication. Solution processable alternatives like graphene oxide (GO) [25,26] are attracting interest due to their various advantages.

Herewith we show synthesis of solution processable BiI_3 nanosheets and effectively demonstrated as hole transport layer (HTL) for OPVs. BiI_3 is a layered semiconducting material having a wide band gap (ca. 2 eV) [27–30]; it has potential applications in room-temperature γ-ray detectors [31] and X-ray digital imaging sensors [32]. Recently, appreciable interest has been shown in the optical properties of BiI_3 because of its strong intrinsic optical anisotropy [27,33,34]. BiI_3 adopts a layered structure (Fig. 1) with Bi^{3+} ions establishing six-fold coordination with I^- ions, which adopt non-linear two-fold coordination with I–Bi–I angles close to 90°. The Bi–I bonds are highly ionic with the 6p electrons of the Bi atoms transferred to the I atoms. The I–Bi–I layers are held together through weak van der Waals forces, allowing BiI_3 crystals to be cleaved readily along the [00l] direction; such weak van der Waals bonding does, however, make this material soft and difficult to handle.

2. Experimental

2.1. Chemicals

Sodium tellurite (99%), bismuth(III) nitrate pentahydrate (99.99%), iodine (99.99%), polyvinylpyrrolidone (PVP; MW=40,000), ethylene glycol (EG, 99%), hydrazine monohydrate (64–65%), acetic acid (99.7%), isopropanol (99.5%), ethanol (99.99%), and acetone (99.9%) were purchased from Sigma–Aldrich and used without further purification.

2.2. Synthesis of BiI_3 crystals

A solution of $NaTeO_3$ (0.3 M) in EG (5 mL), a solution of $Bi(NO_3)_3 \cdot 9H_2O$ (0.3 M) in EG (3.5 mL), PVP (0.5 g), acetic acid (3 mL), and hydrazine monohydrate (0.5 mL) were added to EG (50 mL) and stirred for 20 min. The resulting homogeneous solution was transferred to a 100-mL Teflon-lined stainless-steel autoclave. The sealed vessel was then heated at 160 °C for 2 h before cooling to room temperature. Acetone (20 mL) was added and then the product was separated through centrifugation (12,000 rpm, 1 h) and washed several times with a mixture of acetone and ethanol. The final product was dried in an oven at 80 °C overnight. A solution of Bi_2Te_3 (0.1 M) in water (25 mL) and a solution of I_2 (0.6 M) in water (25 mL) were mixed and then stirred for 30 min; the resulting homogeneous solution was transferred to a 100-mL Teflon-lined stainless-steel autoclave. The sealed vessel was then heated at 180 °C for 10 h before cooling to room temperature. Deionized water (100 mL) was added and then the product separated through centrifugation (12,000 rpm, 1 h) and washed several times with a mixture of water and ethanol (75:25 mL). The final product was dried in an oven at 80 °C overnight.

The synthesis was based on the disproportionation of I_2:

$$Bi_2Te_3 + 6I_2 + 6H_2O \rightarrow 2BiI_3 + 3H_2Te + 3I_2 + 3H_2O + 3/2O_2 \quad (1)$$

Elementary step

$$6I_2 + 6H_2O \rightarrow 6HI + 6\ HIO \quad (2)$$

$$6\ HIO \rightarrow 3\ I_2 + 3H_2O + 3/2\ O2 \quad (3)$$

$$Bi_2Te_3 + 6\ HI \rightarrow 2BiI_3 + 3H_2Te \quad (4)$$

In the hydrothermal process, the pH of the reaction system decreased to less than 1. Thus, it is believed that single crystals of BiI_3 were soluble in hot water under strong acidic conditions. In addition, the instability of HIO [see Eq. (3)] meant that the reaction did not produce BiOI, consistent with the X-ray diffraction (XRD) data. The influence of the reaction time and temperature on the preparation of crystalline BiI_3 was also investigated; the optimal conditions for the formation of highly crystalline BiI_3 were a temperature of 180–190 °C for 10–15 h. If the reaction temperature was below 170 °C or the reaction time was less than 6 h, the yield of BiI_3 diminished and the as-synthesized BiI_3 was poorly crystalline.

2.3. BiI_3 nanosheets: preparation and characterization

The resultant BiI_3 crystals were dispersed in isopropanol (0.25 wt%) and ground to a fine powder at room temperature using a homemade grinder operated at 2000 rpm for 120 min [35]. The solvent and weight-percentage of BiI_3 crystals were optimized based on device performance (see Figs. S1 and S2 and Tables S1 and S2 in Supplementary information). No surfactant or modifying agents were added during grinding. The resultant suspension containing BiI_3 nanosheets was kept for a long period to check its stability; no further precipitation was observed. Powder XRD patterns were recorded at room temperature—using a Bruker D8 X-ray diffractometer equipped with a diffracted beam monochromator set for Cu Kα radiation ($\lambda = 1.54056$ Å)—in the 2θ range 10–80° with a step size of 0.01655° and step time of 0.4 s. Transmission spectra of the films were measured using a Jacobs V-670 UV–Vis spectrophotometer. Scanning electron microscopy (SEM) images were recorded using an FEI Noval 200 scanning electron microscope (15 kV). X-ray photoelectron spectroscopy (XPS) was performed using a PHI 5000 Versa Probe equipped with an Al Kα X-ray source (1486.6 eV). Atomic force microscopy (AFM) images of spin-coated BiI_3 films were recorded using a Vecco di Innova instrument operated in the tapping mode.

2.4. Device fabrication and characterization

ITO-Coated glass substrates ($< 10\ \Omega\ sq^{-1}$, RiTdisplay) were cleaned through ultrasonication—once in detergent (20 min) and subsequently twice in deionized (DI) water (20 min each)—and then dried under N_2 gas and before placing in an oven overnight.

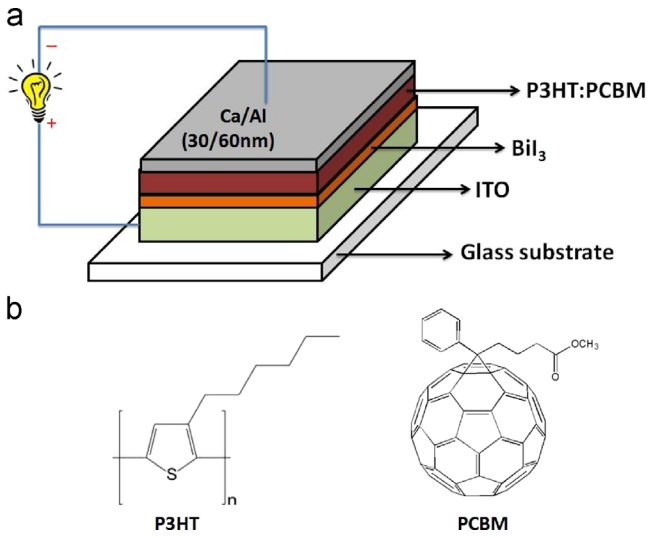

Fig. 2. (a) Schematic representation of the device structure of a fabricated solar cell. (b) Chemical structures of P3HT and PCBM.

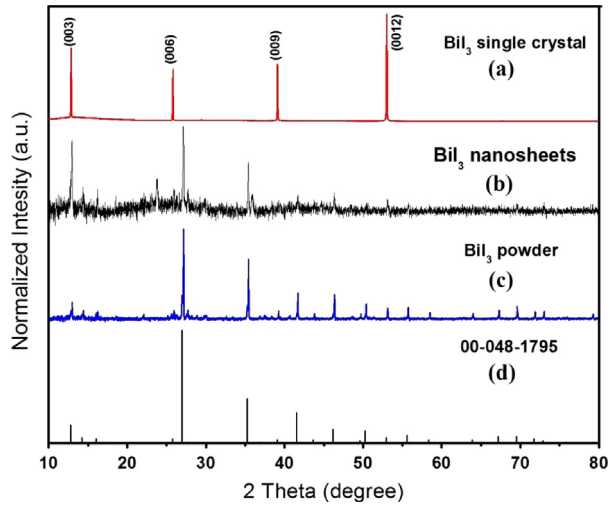

Fig. 3. XRD patterns of the as-prepared BiI_3 single crystals, nanosheets, powder and the BiI_3 standard.

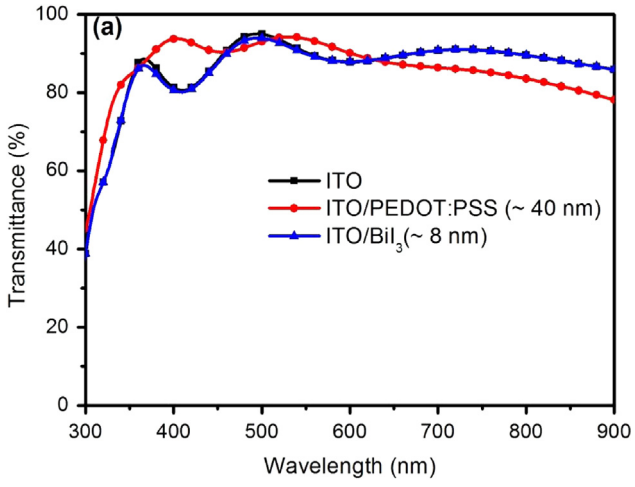

Fig. 4. Transmission spectra of bare ITO and of ITO coated with layers of BiI_3 and PEDOT:PSS.

Immediately prior to spin-coating of the BiI_3 layer, the substrates were treated with ultraviolet (UV)/ozone for 15 min to clean the surfaces and also to improve the surface adhesion. BiI_3 nanosheets were spin-coated onto the ITO surfaces at different spin speeds (1000–5000 rpm) for 1 min and then annealed at 100 °C for 30 min. The nanosheet-coated substrates were transferred to a glove box for coating with the active layer. A blend of P3HT:PCBM (1:1) in 1,2-dichlorobenzene (DCB) was spin-coated (600 rpm, 1 min) to form a thin film (ca. 200 nm) of the active layer. The active layer-coated substrates were kept under a Petri glass dish for 30 min for controlled solvent evaporation and then they were placed on hot plate for thermal annealing at 130 °C for 30 min. To complete the structure of the device (Fig. 2), the top contact was formed through sequential thermal evaporation of Ca (30 nm) and Al (60 nm) through a shadow mask under vacuum (pressure: 1×10^{-6} Torr). The active area of each device was 10 mm^2.

The devices were illuminated with a solar simulator (Thermal Oriel 1000 W), which provided a simulated AM 1.5 spectrum (100 mW cm^{-2}), inside a glove box using a Xe lamp. The light intensity was calibrated using a mono-silicon photodiode with a KG-5 color filter (Hamamatsu). Devices were encapsulated in transparent glass using UV gel and treated with UV light to prevent oxidation during the measurement of the external quantum efficiency (EQE). The EQE spectra were recorded under short-circuit conditions; the light source was a 450-W Xe lamp (Oriel Instruments, model 6123NS). The light output from the monochromator (Oriel Instruments, model 74100) was focused on the photovoltaic cell and the EQE curve was measured.

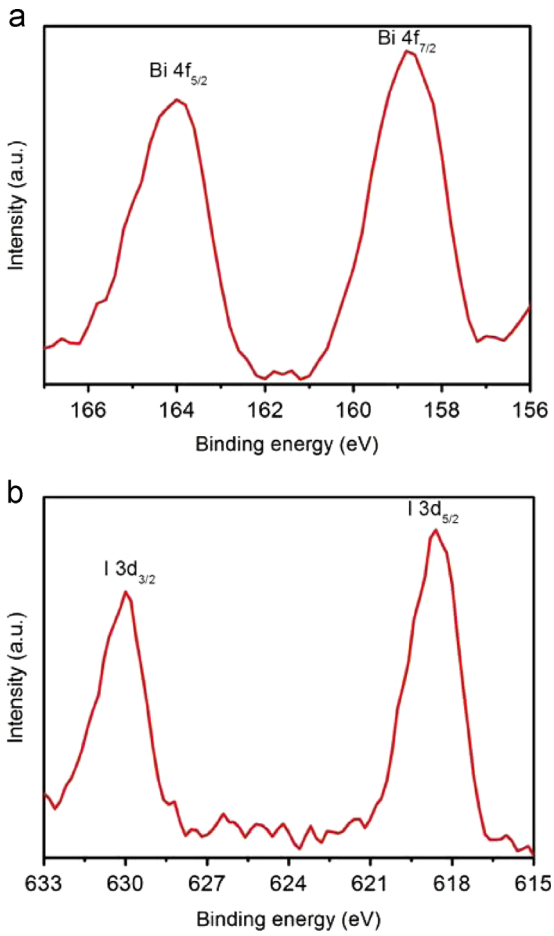

Fig. 5. XPS spectra of a spin-coated BiI_3 film on a glass substrate: (a) Bi 4f and (b) I 3d.

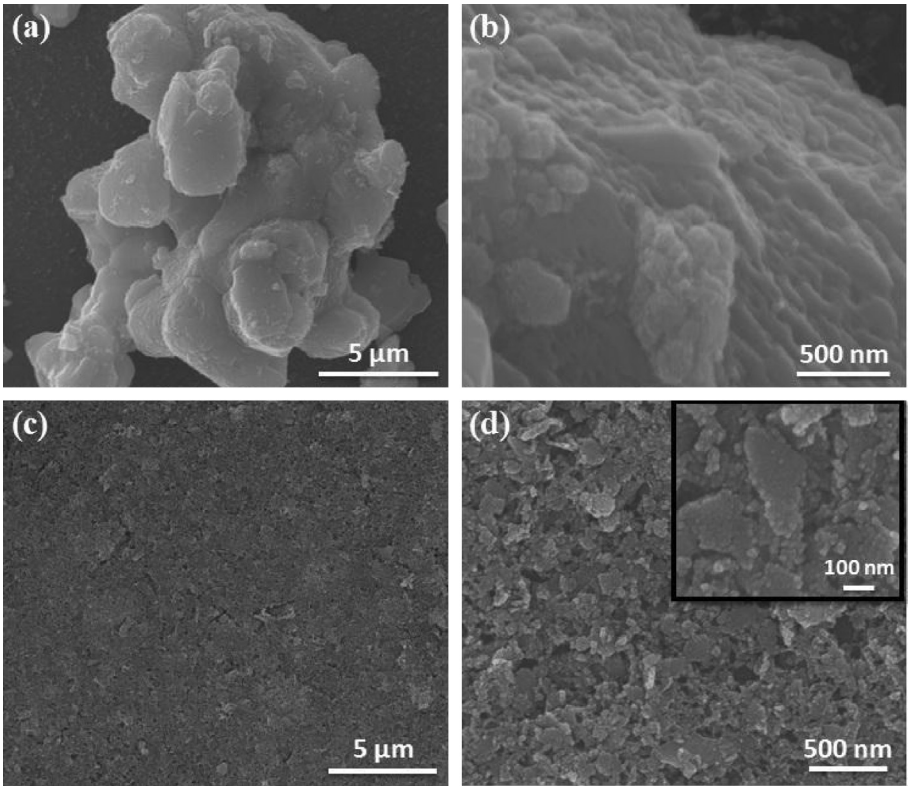

Fig. 6. SEM images of BiI_3 on glass substrates: (a,b) before grinding and (c, d) after grinding.

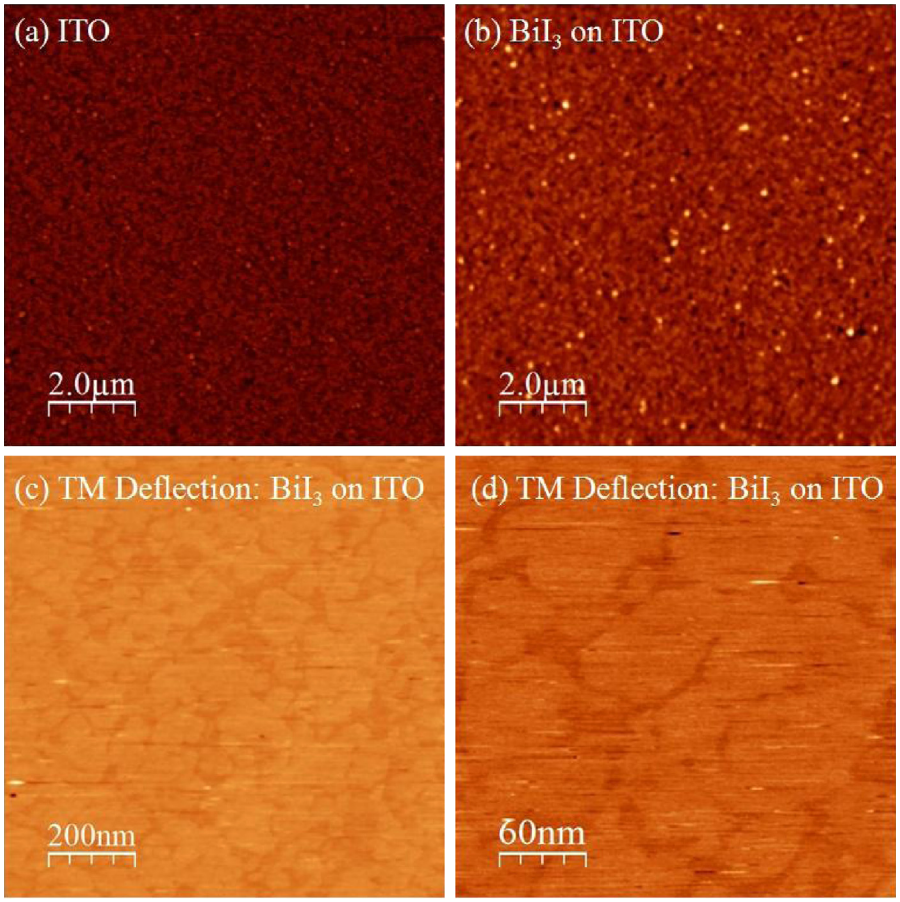

Fig. 7. AFM images of (a) bare ITO and (b) the BiI_3 layer on ITO. (c, d) TM deflection images of a BiI_3 layer on ITO at low and high magnification.

3. Results and discussion

Fig. 3(a) presents a single-crystal XRD pattern indicating that the BiI_3 material crystallized in a single phase that could be indexed to a space group of rhombohedral R-3 structural symmetry with cell parameters (a=7.519 Å; c=20.720 Å) in good agreement with published results [36].

Fig. 3(b) shows the room-temperature powder XRD pattern of BiI_3 nanosheets prepared by homemade wet grinder; all the peaks are indexed with reference data (JCPDS, No. 00-048-1795), no impurity phase present in the exfoliated BiI_3 nanosheets. Fig. 3(c) displays the room-temperature powder XRD pattern of a powder sample obtained using the hydrothermal method; all of the signals in this pattern can be indexed to a hexagonal structure, with no traces of any impurities. We refined the structural parameters using the Rietveld technique with quality refinement parameters. The refined lattice parameters (a=7.525 Å; c=20.710 Å) were consistent with the values reported in the literature (JCPDS, No. 00-048-1795). We detected no impurities (e.g., BiOI). Each unit cell consists of three I–Bi–I layers stacked along the [00l] direction; within each I–Bi–I layer, three close-packed atomic sheets are stacked in the sequence I–Bi–I [34]. Because stacking of the layers is rarely perfect, stacking faults are commonly found in BiI_3 crystals [37,38].

Fig. 4 displays transmission spectra of bare ITO, PEDOT:PSS-coated ITO, and BiI_3-coated ITO. Among these systems, the PEDOT:PSS-coated ITO exhibited the highest optical transmittance in the range 380–500 nm because the smoothness of the ITO surfaces increased after modification with the PEDOT:PSS (~40 nm) layer. The solution-processed BiI_3 (~8 nm) layer on the ITO was highly transparent in the visible region; its transparency was better than that of the PEDOT:PSS-coated ITO in the range 620–900 nm. The highly transparent BiI_3 layer might, therefore, have various applications as an active layer material that can absorb near-IR wavelengths and, thereby, improve device performance.

We recorded XPS spectra to measure the elemental composition and surface characteristics of the BiI_3 film. The XPS survey spectrum of the BiI_3 film contained predominant peaks for Bi and I atoms along with peaks representing Si, C, and O elements (see Fig. S3, Supplementary information). We attribute the XPS peak centered at a binding energy of 284 eV to adventitious hydrocarbon (C 1s) arising from the XPS instrument. The strong signals for O and Si atoms in the XPS spectrum emanated from the glass substrate; no other impurities were evident in the film, in good agreement with the XRD data. Fig. 5 reveals the Bi $4f_{7/2}$ and $4f_{5/2}$ peaks (at 158.8 and 164 eV, respectively) and I $3d_{5/2}$ and $3d_{3/2}$ peaks (at 618.6 and 630 eV, respectively) that are characteristic of Bi^{3+} and I^- species, respectively. Taken together, these results confirm that a stoichiometric BiI_3 film was formed on the substrate.

We prepared samples for SEM characterization by drop-coating BiI_3 onto a glass substrate and then further annealing the system at 100 °C for 15 min, followed by sputtering with gold. We recorded SEM images of the samples obtained before and after grinding the BiI_3 crystals. Fig. 6(a) and (b) displays images of the samples incorporating the non-ground bulk BiI_3 crystals; they reveal layered structures stacked one over another. Similarly, Fig. 6(c) and (d) presents the structures of the samples prepared using the ground sample, revealing fine textured sheets that formed a smooth film on the substrate. The stacked BiI_3 layers were separated and formed nanosheets as a result of shear stresses and mechanical forces during the wet milling process.

We spin-coated (4000 rpm) the BiI_3 nanosheets onto UV-O_3 pretreated ITO-coated glass substrates and then annealed them at 100 °C for 30 min. Fig. 7(a) and (b) presents AFM images of the bare ITO and the BiI_3-modified ITO, respectively. Initially, the root mean square (rms) roughness of the ITO surface was 3.69 nm; it decreased to 2.6 nm after modification with the BiI_3 film. Such an increase in smoothness would tend to decrease the surface scattering of the irradiated light flux from the device. The Tapping Mode (TM) deflection images of the BiI_3-modified ITO in Fig. 7(c) (low magnification) and (d) (high magnification) suggest quite uniform coverage of the BiI_3 nanosheets on ITO.

We fabricated devices having the structure glass/ITO/BiI_3/P3HT:PCBM/Ca/Al (see Fig. 2) for further investigation of the photovoltaic performance and the EQE when using BiI_3 as the HTL. We recorded the J–V characteristics of P3HT:PCBM OPVs prepared with BiI_3 (0.25 wt% in isopropanol) deposited at various spin speeds (1000–5000 rpm) to investigate the effect of the thickness of the BiI_3 layer on the device performance [Fig. 8(a)] under light from a solar simulator operated at 100 mW cm^{-2} (AM 1.5G). Table 1 lists the corresponding device parameters.

Among all of the tested systems, the device incorporating the BiI_3 layer spin-coated at 4000 rpm exhibited the highest PCE (ca. 3.5%), with an open-circuit voltage (V_{oc}) of 0.56 V, a short-circuit current density (J_{sc}) of 10.4 mA cm^{-2}, and a fill factor (FF) of 60.10%. A traditional OPV containing PEDOT:PSS as the HTL exhibited a PCE of approximately 3.83%, with a value of V_{oc} of 0.60 V, a value of J_{sc} of 10.09 mA cm^{-2}, and a FF of 63.26%. Thus, the PCE of the device featuring the BiI_3 layer was comparable with that of the device containing the PEDOT:PSS buffer layer. Increasing the thickness of the BiI_3 layer led to relative decreases in the value of J_{sc} and the PCE (Table 1). The limiting performance was reached at a spin speed of 4000 rpm; thereafter, increasing the spin speed degraded the device performance, possibly because of erosion of

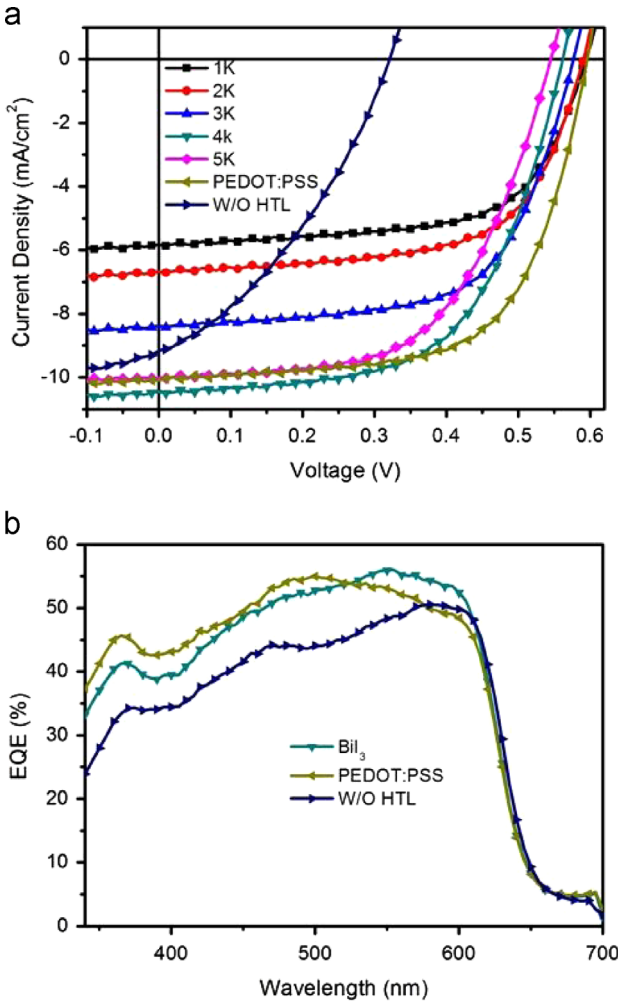

Fig. 8. (a) J–V characteristics of devices incorporating BiI_3 as the HTL layer, deposited at various spin rates. (b) EQE spectra of devices prepared with (BiI_3 or PEDOT:PSS) or without HTLs.

Table 1
Detailed parameters of the performance of devices incorporating BiI_3 HTLs deposited at various spin rates, incorporating PEDOT:PSS as the HTL, and prepared without an HTL.

Spin rate (rpm)	V_{oc} (V)	J_{sc} (mA cm^{-2})	FF (%)	PCE (%)
1000	0.59	5.83	63.95	2.20
2000	0.59	6.67	63.02	2.48
3000	0.58	8.38	62.75	3.05
4000	0.56	10.40	60.10	3.50
5000	0.55	10.01	57.40	3.16
PEDOT:PSS	0.60	10.09	63.26	3.83
W/O HTL	0.32	9.15	36.20	1.06

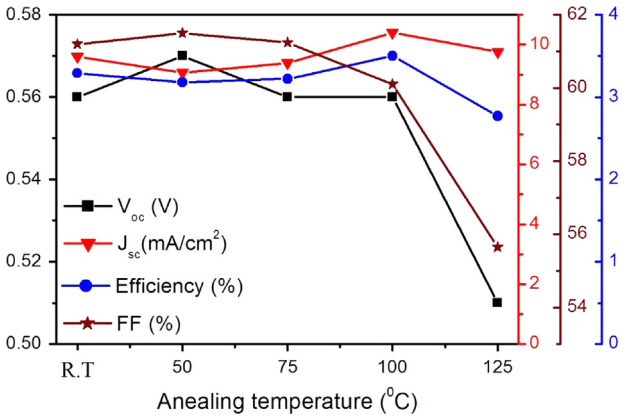

Fig. 9. *J–V* characteristics of photovoltaic devices incorporating BiI_3 as the HTL layer, annealed at various temperatures.

the BiI_3 layer on the ITO surface. To confirm whether the BiI_3 layer functioned as an efficient HTL, we prepared a device in which we spin-coated the active layer directly onto the ITO surface. The poor PCE (ca. 1.06%), with a value of V_{oc} of 0.32 V, a value of J_{sc} of 9.15 mA cm^{-2}, and a FF of 36.20%, confirmed that the BiI_3 nanosheets did indeed play an effective role, forming an efficient HTL between the ITO and the active layer.

Fig. 8(b) presents EQE spectra of solar cells featuring a BiI_3 or PEDOT:PSS layer, or no HTL. Among these systems, the maximum EQE (56%) was reached at a wavelength of 555 nm for the device incorporating the BiI_3 layer deposited at a spin rate of 4000 rpm. The maximum EQE for the PEDOT:PSS-containing device was 55% at 500 nm, while that for the device lacking an HTL was 50.5% at 580 nm. The EQEs of the PEDOT:PSS-modified device were better than those of the BiI_3-modified device within the wavelength range 300–500 nm; above 500 nm, however, the BiI_3-modified device was more efficient. These results are consistent with the transmittance of each material in Fig. 4.

Fig. 9 displays the dependence of the device performance on the annealing temperature. All the samples were annealed for 30 min in air atmosphere. Although we observed no appreciable variations in PCE for the devices prepared with or without annealing, the PCE of the device obtained after annealing at 100 °C was greater than those treated at other annealing temperatures. For annealing temperatures above 100 °C, the PCEs of devices decreased because the thin BiI_3 nanosheets were less stable on the substrate. Accordingly, BiI_3 nanosheets appear to be useful materials for preparing flexible substrates at low temperatures.

4. Conclusion

We have demonstrated that solution-processable BiI_3 nanosheets can be used as HTLs in conventional OPV devices. We synthesized BiI_3 crystals through hydrothermal processing and then ground them using a simple and cost-effective wet milling method to form the BiI_3 nanosheets. We optimized the efficiency by varying the thickness of the BiI_3 nanosheets HTL, the concentration of BiI_3 in the solution used for spin-coating, as well as the annealing temperature of the HTL. The low-temperature-solution-processed BiI_3 nanosheets appear to be compatible with organic materials, suggesting their applicability in various organic electronics.

Acknowledgments

We thank Mr. Hua-Yang Liao and Professor Jing-Jong Shyue (RCAS, Academia Sinica) for help with the SEM and XPS measurements and Mr. Ankur Anand (IAMS, Academia Sinica) for help with the preparation of this manuscript. C.-W.C. thanks the National Science Council (NSC), Taiwan (NSC101-2221-E-001–010, NSC101-2120-M-009-001), Ministry of Education of Taiwan (through the ATU program) and the Thematic Project of Academia Sinica, Taiwan (AS-100-TP-A05), for financial support.

Appendix A. Supplementary information

Supplementary data associated with this article can be found in the online version at http://dx.doi.org/10.1016/j.solmat.2013.10.031.

References

[1] C.-C. Chen, L. Dou, R. Zhu, C.-H. Chung, T.-B. Song, Y.B. Zheng, S. Hawks, G. Li, P.S. Weiss, Y. Yang, Visibly transparent polymer solar cells produced by solution processing, ACS Nano 6 (8) (2012) 7185–7190.
[2] C.J. Brabec, N.S. Sariciftci, J.C. Hummelen, Plastic solar cells, Adv. Funct. Mater. 11 (1) (2001) 15–26.
[3] R. Zhu, C.-H. Chung, K.C. Cha, W. Yang, Y.B. Zheng, H. Zhou, T.-B. Song, C.-C. Chen, P.S. Weiss, G. Li, Y. Yang, Fused silver nanowires with metal oxide nanoparticles and organic polymers for highly transparent conductors, ACS Nano 5 (12) (2011) 9877–9882.
[4] F.C. Krebs, M. Jorgensen, K. Norrman, O. Hagemann, J. Alstrup, T.D. Nielsen, J. Fyenbo, K. Larsen, J. Kristensen, A complete process for production of flexible large area polymer solar cells entirely using screen printing: First public demonstration, Sol. Energy Mater. Sol. Cells 93 (4) (2009) 422–441.
[5] F.C. Krebs, Air stable polymer photovoltaics based on a process free from vacuum steps and fullerenes, Sol. Energy Mater. Sol. Cells 92 (7) (2008) 715–726.
[6] S.-I. Na, B.-K. Yu, S.-S. Kim, D. Vak, T.-S. Kim, J.-S. Yeo, D.-Y. Kim, Fully spray coated ITO-free organic solar cells for low-cost power generation, Sol. Energy Mater. Sol. Cells 94 (8) (2010) 1333–1337.
[7] G. Dennler, M.C. Scharber, C.J. Brabec, Polymer-fullerene bulk heterojunction solar cells, Adv. Mater. 21 (13) (2009) 1323–1338.
[8] B.C. Thompson, J.M. Frechet, Polymer-fullerene composite solar cells, Angew. Chem. Int. Ed. 47 (1) (2008) 58–77.
[9] R. Po, C. Carbonera, A. Bernardi, N. Camaioni, The role of buffer layers in polymer solar cells, Energy Environ. Sci. 4 (2011) 285–310.
[10] S. Chen, J.R. Manders, S.-W. Tsang, F. So, Metal oxides for interface engineering in polymer solar cells, J. Mater. Chem. 22 (2012) 24202–24212.
[11] R. Steim, F.R. Kogler, C.J. Brabec, Interface materials for organic solar cells, J. Mater. Chem. 20 (2010) 2499–2512.
[12] S.H. Eom, S. Senthilarasu, P. Uthirakumar, S.C. Yoon, J. Lim, C. Lee, H.S. Lim, J. Lee, S.-H. Lee, Polymer solar cells based on inkjet-printed PEDOT:PSS layer, Org. Electron. 10 (3) (2009) 536–542.
[13] B. Friedel, P.E. Keivanidis, T.J.K. Brenner, A. Abrusci, C.R. McNeill, R.H. Friend, N.C. Greenham, Effects of layer thickness and annealing of PEDOT:PSS layers in organic photodetectors, Macromolecules 42 (17) (2009) 6741–6747.
[14] H.-Y. Wei, J.-H. Huang, C.-Y. Hsu, F.-C. Chang, K.-C. Ho, C.-W. Chu, Organic solar cells featuring nanobowl structures, Energy Environ. Sci. 6 (2013) 1192–1198.
[15] D. Alemu, H.-Y. Wei, K.-C. Ho, C.-W. Chu, Highly conductive PEDOT:PSS electrode by simple film treatment with methanol for ITO-free polymer solar cells, Energy Environ. Sci. 5 (2012) 9662–9671.
[16] M.P. de Jong, L.J. van IJzendoorn, M.J.A. de Voigt, Stability of the interface between indium-tin-oxide and poly(3,4-ethylenedioxythiophene)/poly(styrenesulfonate) in polymer light-emitting diodes, Appl. Phys. Lett. 77 (14) (2000) 2255–2257.
[17] T. Nguyen, S. de Vos, An investigation into the effect of chemical and thermal treatments on the structural changes of poly(3,4-ethylenedioxythiophene)/polystyrenesulfonate and consequences on its use on indium tin oxide substrates, Appl. Surf. Sci. 221 (2004) 330–339.

[18] T. Stubhan, N. Li, N.A. Luechinger, S.C. Halim, G.J. Matt, C.J. Brabec, High fill factor polymer solar cells incorporating a low temperature solution processed WO_3 hole extraction layer, Adv, Energy Mater. 2 (12) (2012) 1433–1438.
[19] N. Li, T. Stubhan, N.A. Luechinger, S.C. Halim, G.J. Matt, T. Ameri, C.J. Brabec, Inverted structure organic photovoltaic devices employing a low temperature solution processed WO_3 anode buffer layer, Org. Electron. 13 (11) (2012) 2479–2484.
[20] J.-H. Huang, T.-Y. Huang, H.-Y. Wei, K.-C. Ho, C.-W. Chu, Wet-milled transition metal oxide nanoparticles as buffer layers for bulk heterojunction solar cells, RSC Adv. 2 (2012) 7487–7491.
[21] S. Murase, Y. Yang, Solution processed MoO_3 interfacial layer for organic photovoltaics prepared by a facile synthesis method, Adv. Mater. 24 (18) (2012) 2459–2462.
[22] Y.-J. Lee, J. Yi, G.F. Gao, H. Koerner, K. Park, J. Wang, K. Luo, R.A. Vaia, J.W.P. Hsu, Low-temperature solution-processed molybdenum oxide nanoparticle hole transport layers for organic photovoltaic devices, Adv. Energy Mater. 2 (10) (2012) 1193–1197.
[23] E.L. Ratcliff, J. Meyer, K.X. Steirer, A. Garcia, J.J. Berry, D.S. Ginley, D.C. Olson, A. Kahn, N.R. Armstrong, Evidence for near surface NiOOH species in solution-processed NiO_x selective interlayer materials: impact on energetics and the performance of polymer bulk heterojunction photovoltaics, Chem. Mater., 23, 4988–5000.
[24] C. Gong, H.B. Yang, Q.L. Song, C.M. Li, Nanostructure effect of V_2O_5 buffer layer on performance of polymer-fullerene devices, Org. Electron. 13 (1) (2012) 7–12.
[25] J.-M. Yun, J.-S. Yeo, J. Kim, H.-G. Jeong, D.-Y. Kim, Y.-J. Noh, S.-S. Kim, B.-C. Ku, S.-I. Na, Solution-processable reduced graphene oxide as a novel alternative to PEDOT:PSS hole transport layers for highly efficient and stable polymer solar cells, Adv. Mater. 23 (42) (2011) 4923–4928.
[26] J. Liu, Y. Xue, Y. Gao, D. Yu, M. Durstock, L. Dai, Hole and electron extraction layers based on graphene oxide derivatives for high performance bulk heterojunction solar cells, Adv. Mater. 24 (17) (2012) 2228–2233.
[27] E. Lifshitz, L. Bykov, Continuous-wave, microwave-modulated, and thermal-modulated photoluminescence studies of the BiI_3 layered semiconductor, J. Phys. Chem. 99 (14) (1995) 4894–4899.
[28] J. Bordas, J. Robertson, A. Jakobsson, Ultraviolet properties and band structure of SnS_2, $SnSe_2$, CdI_2, PbI_2, BiI_3 and BiOI crystals, J. Phys. C: Solid State Phys. 11 (12) (1978) 2607–2621.
[29] G.E. Jellison, J.O. Ramey, L.A. Boatner, Optical functions of BiI_3 as measured by generalized ellipsometry, Phys. Rev. B 59 (1999) 9718–9721.
[30] H. Yorikawa, S. Muramatsu, Theoretical study of crystal and electronic structures of BiI_3, J. Phys.: Condens. Matter. 20 (32) (2008) 325220.
[31] D. Nason, L. Keller, The growth and crystallography of bismuth triiodide crystals grown by vapor transport, J. Cryst. Growth 156 (3) (1995) 221–226.
[32] A.T. Lintereur, W. Qiu, J.C. Nino, J.E. Baciak, Bismuth tri-iodide radiation detector development, Proc. SPIE 7449 (2009) 74491M_1–74491M_7.
[33] V. Agekyan, Growth and optical properties of BiI_3 and PbI_2 microcrystals, Phys. Solid State 40 (9) (1998) 1568–1573.
[34] X.-X. Sun, Y.-L. Li, G.-H. Zhong, H.-P. Lu, Z. Zeng, The structural, elastic and electronic properties of BiI_3: first-principles calculations, Physica B 407 (4) (2012) 735–739.
[35] M.A. Ibrahem, H.-Y. Wei, M.-H. Tsai, K.-C. Ho, J.-J. Shyue, C.W. Chu, Solution-processed zinc oxide nanoparticles as interlayer materials for inverted organic solar cells, Sol. Energy Mater. Sol. Cells 108 (2013) 156–163.
[36] A. Matsumoto, K. Hitomi, T. Shoji, Y. Hiratate, Bismuth iodide (III) crystals for nuclear radiation detectors, in: Nuclear Science Symposium Conference Record, 2001 IEEE, vol. 4, 2001, pp. 2344–2347.
[37] Y. Kaifu, Excitons in layered BiI_3 single crystals, J. Lumin. 42 (2) (1988) 61–81.
[38] T. Karasawa, T. Kawai, I. Akai, Y. Kaifu, Observation of highly mobile exciton along the stacking fault plane in BiI_3 by space-resolved spectroscopy, J. Lumin. 40–41 (1988) 431–432.